PROCESS SIMULATION AND OPTIMISATION OF H₂ PRODUCTION FROM ETHANOL STEAM REFORMING AND ITS USE IN FUEL CELLS.

2. Process analysis and optimisation.

Ilenia Rossetti[1], Matteo Compagnoni and Mauro Torli

Dip. Chimica, Università degli Studi di Milano, INSTM Unit Milano-Università and CNR-ISTM, via Golgi 19, 20133 Milano, Italy

ABSTRACT

The feasibility of power cogeneration through fuel cells using bioethanol with different concentration has been considered. Data and layout have been inspired by an existing unit Helbio, GH2 -BE- 5000 (5 $kW_{electrical}$ + 5 $kW_{thermal}$) system for combined heat and power generation (CHP). The system is constituted by six reactors connected in series for hydrogen production and purification and by a fuel cell of the mentioned capacity.

To evaluate process efficiency and the possibility to operate with diluted bioethanol feed, characterized by lower purification cost, different process layouts have been tested. Particular attention is paid to the intensification of the heat exchange network, to increase the overall plant efficiency. Heat supply to the steam reformer has been accomplished by burning part of the reformate, since diluted ethanol is not suitable to feed the burner as in the experimental process layout.

The water/ethanol feeding ratio has been taken as major parameter for simulation. An increase of this variable improved H₂ yield due to promotion of the water gas shift reaction and lower impact of the hydrogen-consuming methanation step. However, higher heat input was required by the reformer, implying the delivery of a higher fraction of the reformate to

---

[1] Corresponding author: fax 0039-02-50314300; email ilenia.rossetti@unimi.it

the burner instead than to the fuel cell. This means lower electric output and efficiency. However, the presence of a high enthalpy steam exhaust increased the available thermal output, with consequent increase of the thermal and overall efficiency of the plant.

1 - INTRODUCTION

In order to find out alternative routes for the co-generation of heat and power (CHP) from renewable sources, different strategies have been proposed. Among these, H_2 production from bioethanol, coupled to fuel cells raised considerable attention in recent years [1-3]. In addition, highly innovative solutions for the production of second generation biofuels are becoming available, leading to environmentally, ethically and economically sustainable bioethanol. The economical plan proposed by Biochemtex, for instance, is based on 0.3 euro/L for the production of lignocellulosic anhydrous bioethanol [4].

A 250 W system based on authothermal reformer and a fuel cell stack has been studied [5]. A minimum amount of process controls and little internal heat integration kept system architecture simple, as required for portable applications, at difference with the presently studied system, in which heat integration was part of the optimization. Indeed, for stationary applications the increase of efficiency is seen as a predominant factor with respect to simplification.

A similar system has been proposed, with reformate purification from CO based on preferential oxidation and attention to the control logic and heat integration [6-8]. On a completely different scale, the technical feasibility of using existing steam reforming and hydrogen separation technologies to produce hydrogen from bioethanol at industrial level (100,000 Nm^3/h) has been explored [9]. The product distribution in a steam reformer as a function of water/ethanol feeding ratio, possibly including a carrier gas, has been simulated

[10]. Moreover, very recently thermodynamic analysis and process simulation of a reactor producing reformate by oxidative reforming of n-butanol has been carried out [11], coupled with an experimental study on oxidative reforming of ethanol [12] and n-hexadecane [13] in microreactors to feed micro-fuel cell systems. Computational fluid dynamics simulation of ethanol steam reforming in catalytic wall microchannels has been performed on a Co_3O_4-ZnO catalyst [14].

Membrane reactors also attracted attention for similar applications [15-17]. Structured membranes can allow significant H_2 purification from CO and CO_2.

More in general, a typical layout of a CHP system is composed of:

♣ A multi-tubular reactor filled with an ethanol steam reforming (SRE) catalyst. The heat of reaction is provided on the outer wall of the tubes by combustion of part of the reactant (C_2H_5OH with high concentration), as described e.g. in [18]. It is alternatively possible to use part of the reformate from the reactor or a portion of the H_2 produced [19]. The most innovative designs provide a catalytic burner, the catalysts for the catalytic combustion of C_2H_5OH being coated on the outer surface of the reformer tubes, in very efficient thermal contact with the reforming catalyst which is coated on the internal skin of the same tubes [20]. Different possible configurations strictly depend on the size of the system. Another solution, feasible only with high temperature fuel cells, such as the solid oxide ones, proposes the use of the stack effluent to heat up the reforming reactor. A further possibility is the use of an afterburner for the Fuel Cell (FC) effluent [21] or the use of molten salts as thermal vector [22]. Alternatives for the SRE reactor may be a unit for ethanol dehydrogenation to acetaldehyde, followed by reforming of the latter [23] or autothermal reformers. A multichannel reactor has been also considered in the literature, with detailed modeling [24].

♣ Water Gas Shift (WGS) reactors in variable number to ensure proper H_2 yield and reformate purification from CO. Typically, a first reactor aims at increasing H_2 yield and it is

usually operated at relatively high temperature (350-400°C). WGS is an exothermal reaction and under these conditions *ca.* 90% of the CO outflowing from the SRE reactor may be converted to CO_2. Subsequent reactor(s), working at decreasing temperatures, abate CO concentration in the reformate to meet the specifications of the fuel cell. The catalysts are usually based on Fe -Cr oxides for the high temperature stage (HT-WGS) and Cu- ZnO for the low temperature one (LT-WGS) [25].

♣ A preferential oxidation (PROX) reactor, or, alternatively, a selective methanation (METH) reactor is commonly added if fuel cells operating at low temperature are used. The purpose of these units is to reduce the content of CO in the reformate below 20 ppm, *i.e.* the threshold CO tolerance of a Polymer Electrolite Membrane FC (PEMFC). However, both options present some drawbacks. In the case of PROX [26]

$$2CO + O_2 \rightarrow 2CO_2 \qquad\qquad\qquad (R1)$$

O_2 demand is usually overstoichiometric leading to some H_2 depletion. Moreover, inert N_2 coming from air further dilutes the reformate. By contrast, in the case of METH [27]

$$CO + 3H_2 \leftrightarrow CH_4 + H_2O \qquad\qquad\qquad (R2)$$

the consumption of H_2 depends on residual CO amount in the reformate. In these units the parallel methanation of CO_2 may also occur. The latter reaction may be keep under control by tuning catalyst selectivity and operating temperature (*ca.* 200-215°C). In addition, the low CO concentration may favor the reverse WGS with sudden methanation of the CO thus formed [28]. The most commonly used methanation catalysts are based on Ni, Ru or Rh supported over oxides (*e.g.* alumina). Another possible alternative may be the physical

separation of CO by Pressure Swing Adsorption (PSA), which is however indicated when pressure gradients are significant and admitted.

♣ A stack of FC: usually PEMFC, also as new HT-PEMFC (High Temperature PEMFC), SOFC (Solid Oxide FC) or MCFC (Molten Carbonate FC). These cells have widely different operating temperatures and they allow operation with increasing amounts of CO (from ppm to percent), in the order: 60-80°C, 160-180°C, 800-1000°C and 650-800°C. Therefore, according to the type of FC, the number of WGS units ranges from 1 to 3 and PROX/METH reactors may be unnecessary.

The main purpose of this work is to quantify the electric power and thermal energy output, as well as the overall efficiency of a plant for CHP with residential size (5 kW$_{electrical}$ + 5 kW$_{thermal}$). In particular, the system is based on a PEMFC, fed with reformate produced by steam reforming of bioethanol. Reformate purification from CO is accomplished by a series of WGS and METH reactors. Different tools have been used, such as Aspen Plus$^©$, Matlab$^©$, Athena Visual Studio$^©$ for process simulation and analysis. The operational variables chosen for the simulation are taken by an actually existing unit GH2 -BE- 5000 (Helbio SA, Hydrogen and Energy Production Systems), better described in the following and capable of delivering the required output [18,29]. The thermodynamic and kinetic input data have been selected as detailed in the first part of this work, in particular by using Model 3.
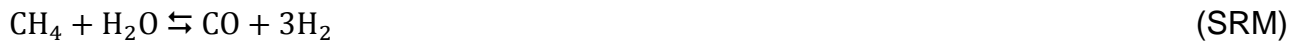
Among the different operating variables considered, the water/ethanol ratio was found particularly relevant to optimise process yield and its economic sustainability.

2 –MODELS AND METHODS

2.1 – Kinetic model

A detailed revision of kinetic models available was necessary, since process simulation including reactor sizing in the case of the steam reforming reactor requires a suitable reaction scheme with the relative kinetic parameters. Therefore, the kinetic model has been adapted from literature as extensively described in part 1, and labelled as *Model 3*. Briefly, such model was originally developed for a Rh(1wt%)MgAl$_2$O$_4$/Al$_2$O$_3$ catalyst [30] and includes 14 elementary steps, 4 of which were proposed as rate determining ones.

The following set of rate equations have been proposed for ethanol decomposition (ED), Ethanol steam reforming (SRE), methane steam reforming (SRM) and water gas shift (WGS):

$$CH_3CH_2OH \rightarrow CH_4 + CO + H_2 \tag{ED}$$

$$CH_3CH_2OH + H_2O \rightarrow CO_2 + CH_4 + 2H_2 \tag{SRE}$$

$$CH_4 + H_2O \leftrightarrows CO + 3H_2 \tag{SRM}$$

$$CO + H_2O \leftrightarrows CO_2 + H_2 \tag{WGS}$$

$$r_{ED} = \frac{k_5 N \frac{[p_{C_2H_5OH}]}{[p_{CH_4}][p_{H_2}]^{0,5}}[C_T]^2}{\left[1+A[p_{C_2H_5OH}]+C\frac{[p_{CH_4}]}{[p_{H_2}]^{0,5}}+F\frac{[p_{H_2O}]}{[p_{H_2}]^{0,5}}+G[p_{CH_4}]+H[p_{CO}]+I[p_{CO_2}]+J[p_{H_2}]^{0,5}+L\frac{[p_{C_2H_5OH}]}{[p_{H_2}]^{0,5}}+M\frac{[p_{C_2H_5OH}]}{[p_{H_2}]}+N\frac{[p_{C_2H_5OH}]}{[p_{CH_4}][p_{H_2}]^{0,5}}\right]^2} \tag{1}$$

$$r_{SRE} = \frac{k_7 NF \frac{[p_{C_2H_5OH}][p_{H_2O}]}{[p_{CH_4}][p_{H_2}]}[C_T]^2}{\left[1+A[p_{C_2H_5OH}]+C\frac{[p_{CH_4}]}{[p_{H_2}]^{0,5}}+F\frac{[p_{H_2O}]}{[p_{H_2}]^{0,5}}+G[p_{CH_4}]+H[p_{CO}]+I[p_{CO_2}]+J[p_{H_2}]^{0,5}+L\frac{[p_{C_2H_5OH}]}{[p_{H_2}]^{0,5}}+M\frac{[p_{C_2H_5OH}]}{[p_{H_2}]}+N\frac{[p_{C_2H_5OH}]}{[p_{CH_4}][p_{H_2}]^{0,5}}\right]^2} \tag{2}$$

$$r_{SRM} = \frac{k_{13} CF \left[\frac{[p_{CH_4}][p_{H_2O}]}{[p_{H_2}]}-\frac{1}{K_{SRM}}[p_{CO}][p_{H_2}]^2\right][C_T]^2}{\left[1+A[p_{C_2H_5OH}]+C\frac{[p_{CH_4}]}{[p_{H_2}]^{0,5}}+F\frac{[p_{H_2O}]}{[p_{H_2}]^{0,5}}+G[p_{CH_4}]+H[p_{CO}]+I[p_{CO_2}]+J[p_{H_2}]^{0,5}+L\frac{[p_{C_2H_5OH}]}{[p_{H_2}]^{0,5}}+M\frac{[p_{C_2H_5OH}]}{[p_{H_2}]}+N\frac{[p_{C_2H_5OH}]}{[p_{CH_4}][p_{H_2}]^{0,5}}\right]^2} \tag{3}$$

$$r_{WGS} = \frac{k_{14} HF \left[\frac{[p_{CO}][p_{H_2O}]}{[p_{H_2}]^{0,5}}-\frac{1}{K_{WGS}}[p_{CO_2}][p_{H_2}]^{0,5}\right][C_T]^2}{\left[1+A[p_{C_2H_5OH}]+C\frac{[p_{CH_4}]}{[p_{H_2}]^{0,5}}+F\frac{[p_{H_2O}]}{[p_{H_2}]^{0,5}}+G[p_{CH_4}]+H[p_{CO}]+I[p_{CO_2}]+J[p_{H_2}]^{0,5}+L\frac{[p_{C_2H_5OH}]}{[p_{H_2}]^{0,5}}+M\frac{[p_{C_2H_5OH}]}{[p_{H_2}]}+N\frac{[p_{C_2H_5OH}]}{[p_{CH_4}][p_{H_2}]^{0,5}}\right]^2} \tag{4}$$

The expressions for the coefficients A-N appearing in the rate equations above are reported in the original paper [30]. The rate expressions for WGS and SRM are much more complex than those usually derived for such reactions. WGS and SRM in this case are not occurring alone on catalyst surface, but they are part of a complex reaction mechanism. Based on a Langmuir Hinshelwood approach, all the species concurring for adsorption over active sites should appear in the denominator of the rate expressions and are included in the overall balance on the active sites, leading to complex rate equations.

This model has been applied by us to a full set of experimental data collected for a Ni/Al_2O_3 sample [31]. This allowed to represent with good accuracy the experimental data, validating the proposed model also for a different catalytic system, and to provide a reliable estimate of the whole set of kinetic parameters needed for the present simulations and for steam reformer reactor sizing, as summarised in Table 1. Indeed, the required data were not fully available in the literature.

2.2 – Layout of the CHP unit

In the present work, we concentrated on a CHP unit Helbio, GH2-BE-5000 [18]. It is composed of a prereformer, a reforming reactor, two units of HT- and LT-WGS and two selective METH reactors, all connected in series. To provide reformate to feed a 5 kW$_{el}$ FC, the plant is fed with 142 g/min of a solution with H_2O/C_2H_5OH = 5.7 mol/mol. Heat supply to the reformer is ensured by the catalytic combustion of 96 vol% C_2H_5OH. The reformate is fed to a PEMFC operating at 80°C and 1.8 bar. A heat recovery system is present to increase the overall process efficiency.

The process flowsheet used in the following simulations has been modified, being based on a single SRE reactor and one METH, since during our experimental testing we have seen that the second METH is only a guard reactor, because the reformate meets the

specifications for CO concentration already after the first one. Additionally, we have redrawn the heating and heat recovery system in order to allow the use of diluted ethanol solutions, unsuitable for the catalytic burner used in the experimental set up.

Therefore, we used reformate to heat up the reformer in the simulated plant. A sketch of the experimentally available layout and of the modified system used for the present simulations is reported in Fig. 1.

For the implementation of process simulations it was necessary to use an appropriate set of kinetic equations and the relative optimised parameters to describe the above processes. These models have been recovered in the literature, while the parameters were obtained by regression of experimental data, as extensively described in part 1 of the present work and summarised in paragraph 2.1.

2.3 – Sizing/rating of the SRE reactor

A continuous downflow tubular reactor has been modelled. A rigorous sizing of the system is out of the scope of the present work. Therefore, the following approximations have been taken into account. According to the possible reactor configuration, catalyst particle size and type and volumetric flow, external (turbulent flow and similar performance with different flow rate at constant contact time) and internal diffusional limitations have been neglected (limited porosity, catalyst efficacy *ca.* 1). Radial and axial temperature and concentration gradients have been neglected, assuming a plug-flow approximation.

The kinetic model defined as *Model 3* in the first part of this work has been selected [30], with the set of kinetic parameters estimated in part 1 and here summarised in Table 1. We recall in the following the material balances for each species and the reaction set used.

$$dn_{CH_3CH_2OH} = v(-r_{ED} - r_{ER})d\tau \qquad\qquad (5)$$

$$dn_{H_2O} = v(-r_{ER} - r_{SRM} - r_{WGS})d\tau \tag{6}$$

$$dn_{H_2} = v(r_{ED} + 2r_{ER} + 3r_{SRM} + r_{WGS})d\tau \tag{7}$$

$$dn_{CO_2} = v(r_{ER} + r_{WGS})d\tau \tag{8}$$

$$dn_{CO} = v(r_{ED} + r_{SRM} - r_{WGS})d\tau \tag{9}$$

$$dn_{CH_4} = v(r_{ED} + r_{ER} - r_{SRM})d\tau \tag{10}$$

Where τ is the contact time, v the volumetric flow rate and r_i the rate of each reaction.

The following thermal balance has been added:

$$v\rho c_p dT_i = dw_Q + [r_{ED}(-\Delta_r H_{ED}) + r_{ER}(-\Delta_r H_{ER}) + r_{SRM}(-\Delta_r H_{SRM}) + r_{WGS}(-\Delta_r H_{WGS})]dV \tag{11}$$

where r is reaction rate, ρ is density and c_p the specific heat at constant pressure of the reacting system at a given axial coordinate; T_i the temperature inside the tubes, dw_Q heat input to the reactor, $(-\Delta_r H_i)$ the reaction enthalpy of each reaction and dV the elementary volume of catalyst bed (correlated to dW, elementary catalyst mass through the known catalyst density). The thermal input/output may be calculated as:

$$dw_Q = U_i \frac{4dV}{D_i}(T_e - T_i) \tag{12}$$

where T_e is the temperature of the heating fluid at the same coordinate, U_i and D_i are the global coefficient of thermal exchange and internal pipe diameter, respectively, while $4dV/D_i$ represents the internal elementary heat exchange surface. Furthermore, the following thermal balance holds for the external heating medium:

$$v_e \rho_e c_{pe} dT_e = -dw_Q \tag{13}$$

The pressure (P) profile along the catalyst bed has been taken into account:

$$dP = \left(\frac{\Delta P_a}{L}\right)\frac{4 dV}{\pi D_i^2}$$

(14)

where $(\Delta P_a/L)$ represents the uniform pressure drop across the bed, which has been calculated according to the Ergun equation [32,33].

Variable GHSV (gas hourly space velocity) values have been used. Referring to ethanol as limiting agent with constant feed and considering the gas volume in normal conditions GHSV was varied between 314 and 7700 h^{-1}.

2.4 - Fuel cell

A PEMFC has been considered. Its efficiency η has been calculated as follows:

$$\eta = \eta_V \eta_I \eta_{max} = \eta_V \eta_I \frac{E_{rev} v_e F}{-\Delta_r H} = \eta_I \frac{E v_e F}{-\Delta_r H}$$

(15)

where η_{max} represents the thermodynamic efficiency, η_V the potential efficiency (taking into account ohmic losses, activation polarization and concentration polarization), η_I the current efficiency. E_{rev} represents the reversible potential of the cell, v_e is the number of equivalents of electrons transferred during the redox reaction, F is the Faraday's constrant and $\Delta_r H$ the enthalpy variation during the same reaction.

No adequate unit operation was available to model the PEMFC in AspenPlus©, so it was treated as reactor for H_2 combustion. The electrical work and heat were calculated from the

enthalpy change across the reactor, by taking into account the efficiency parameters reported for similar systems [34].

3 - RESULTS AND DISCUSSION

3.1. – Flowsheet and parameters to be optimised

Experimental data relative to the existing GH2-BE-5000 unit have been presented elsewhere [18,29]. Testing allowed to validate the integration of the six reactors to accomplish reformate production and purification with the desired flow rate. Satisfactory H_2 purity has been achieved after methanation, CO concentration being well below the threshold of 20 ppm imposed by the PEMFC in use. However, interestingly low CO amount was also obtained after the LT-WGS stage, *i.e.* 0.4 vol%. This allows the direct coupling the fuel processor with a HT-PEMFC, working at high temperature and more tolerant to CO.

The flowsheet of the system is reported in Fig. 2. This conceptually represents the scheme of the experimental system in use, except for the intensification of the heat exchange network and the heat supply, in order to improve the overall efficiency, *i.e.* including the modifications summarised in Fig. 1. Furthermore, the burner which furnished reaction heat to the reformer is represented in Fig. 2 as external unit operation, whereas it is conceived as a catalytic burner located in the shell side of the real reformer in use. Similarly, heat recovery allowed by the heat exchangers EX4, EX6 and EX8 is truly made in the shell side of the two WGS reactors and METH unit. The start up of the unit is allowed by burning an auxiliary fuel, although transient response is not considered in the present work.

The following chemical species have been taken into account C_2H_5OH, H_2O, H_2, CO_2, CO, CH_4, O_2 and N_2. The Peng-Robinson equation of state has been adopted, since it is particularly suited to describe light gas mixtures in a wide temperature and pressure range.

However, negligible differences have been observed by using different thermodynamic packages, except in some cases (*vide infra*).

The feed has been set equal to the experimental value, *i.e.* 44 g min^{-1} (0.92 mol min^{-1}), for C_2H_5OH, whereas the water molar flow has been widely varied between 5 and 14 times the molar flow of ethanol. The steam reformer temperature has been set at 750°C.

The lower limit is imposed by the need to operate overstoichiometrically to promote the WGS reaction and to limit coking. As for the latter parameter we selected the operating window as for temperature and water/ethanol ratio in a conservative way. Indeed, based on our own experience and other literature data, coking can be considered negligible over the most commonly used catalysts when operating at T > 600°C with stoichiometric feeding ratio. Lower temperature is admissible in overstoichiometric water/ethanol conditions. The upper limit is imposed by the heat input needed to fully vaporize the feed: above this limit an additional heater would be necessary.

Fictitious 10^{-8} mol min^{-1} inlet flow of CH_4 and H_2 is imposed by Model 3 as detailed in Part 1. A variation over two order of magnitudes of this value did not affect the calculated concentration profiles, even in the first integration intervals. Air flow to the burner has been set 110% with respect to the stoichiometric need for the fuel (ethanol and/or H_2).

Since part of the reformate is used as fuel to heat the steam reformer, a crucial parameter is the split ratio of the reformate between the burner and the fuel cell. Indeed, on one hand it would be preferable to feed as much as possible the FC, but this would decrease the reformer temperature with the consequent drop of H_2 yield. Therefore, this parameter was optimized and the air flow to the burner and the FC was varied accordingly.

One pump and one compressor are considered and operated so to allow 1.8 bar pressure at FC inlet.

Different heat exchangers are present, allowing fine heat recovery and decreasing the reformate supply to the burner. This is possible because a cascade cooling is compulsory

to decrease stream temperature to *ca.* 80°C before feeding the FC. The configuration of heat exchangers has been always considered countercurrent with a minimum difference of temperature between the fluid streams of 5°C. Particular attention is needed when dealing with heat exchangers characterized by liquid-vapor equilibrium, in particular EX2 and EX3. Indeed, the sizing of the system is usually done by respecting these conditions:

$$H_{h.s.}^{i} - H_{h.s.}^{o} = H_{c.s.}^{o} - H_{c.s.}^{i} \tag{16}$$

$$T_{h.s.}^{i} > T_{c.s.}^{o} \cup T_{h.s.}^{o} > T_{c.s.}^{i} \tag{17}$$

labelling with h.s. and c.s. the hot and cold sides, respectively. In such case, an improper evaluation of the liquid-vapor equilibrium may lead to physically unreliable temperature profiles across the heat exchanger. In these cases, an UNIQUAC model has been found more reliable to predict the behavior of aqueous solutions of ethanol and it has been implemented in the simulation. Similar results have been obtained with the NRTL thermodynamic package implementing the Wilson mixing rule.

Both the WGS reactors and the METH unit have been considered as Gibbs reactors, since the experimental outflowing concentration was always comparable to the equilibrium conversion. The use of equilibrium conditions in this section should not be confused with the use of the WGS reaction rate above described. That was intended as part of the complex reaction set for the modeling of the steam reformer reactor. Here a less complex reaction mixture is present and thermodynamic regime is reached downstream the SR reactor.

Their operating temperatures were set to 350°C for the HT-WGS, 280°C for the LT-WGS and 210°C for the METH reactor, respectively. Literature data represent very limited unselective methanation of CO_2 at 210°C with selective commercial catalysts. Data for a 5%Ru-Al_2O_3 catalyst [28], similar to those employed in our case, report the following

stoichiometry as worst acceptable case in the chosen temperature range and this scenario has been considered as the more pessimistic condition in our simulations:

$$CO + 0,5CO_2 + 5H_2 \rightarrow 1,5CH_4 + 2H_2O \tag{R3}$$
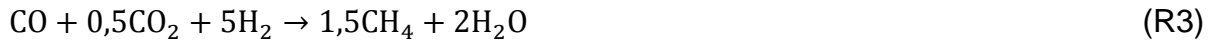
All these reactors have been connected to proper heat-links for heat recovery.

3.2. – Sizing of the SRE unit

More detailed sizing and analysis was done for the reformer reactor and its burner. A multitubular reactor configuration was chosen, with reforming catalyst on tube side and the hot combustion gases on the shell side. The best results were obtained by adopting a co-current configuration, in order to provide higher heat amount in the first catalyst layers, where most reactants are converted. The optimised catalyst particle size was 1.2 mm, allowing to achieve limited intraparticle diffusional limitations and acceptable pressure drop across the catalytic bed. Accordingly, tubes diameter was set *ca*. 10 times larger to avoid by-pass phenomena. Reactor length was set sufficiently long to neglect inlet phenomena, but not too long to increase appreciably pressure drop. The tubes number was varied according to the operating conditions. A summary of one possible configuration is reported in Table 2.

A specific calculation has been carried out to determine the global heat transfer coefficient (U) across the heat exchanger reactor. The resistance to heat transfer across the metallic tubes has been neglected, so that

$$\frac{1}{U} = \frac{1}{h_i} + \frac{1}{h_e} \tag{18}$$

h_i and h_e being the liminar coefficients inside and outside the tubes, respectively. The former term has been calculated through the following equation, adapt to estimate heat transfer between a solid wall and a layer of solid particles [32,33]:

$$h_i = \frac{k}{D_p}\left[0{,}203(RePr)^{1/3} + 0{,}220Re^{0{,}8}Pr^{0{,}4}\right] \tag{19}$$

The Reynolds and Prandtl numbers are calculated as follows:

$$Re = \frac{D_p u_s \rho}{\mu} \tag{20}$$

$$Pr = \frac{c_p \mu}{k} \tag{21}$$

$$u_s = \frac{4v}{n\pi D^2} \tag{22}$$

where k, ρ, c_p and μ are the thermal conductivity, density, heat capacity and viscosity of the fluid (all calculated at the fluid temperature), D_p is particle diameter, v the volumetric flow rate, n the number of tubes in the selected configuration, D tube diameter and u_s the surface velocity (with empty reactor). To calculate the same parameter for the shell side, an additional term for radiative heat transfer (h_r) has been added to the liminar coefficient (h'_e):

$$h_e = h'_e + h_r \tag{23}$$

$$h'_e = \frac{k_e}{D}\left[0{,}25Re^{0{,}6}Pr^{0{,}33}\left(\frac{\mu_e}{\mu_{we}}\right)^{0{,}14}\right] \tag{24}$$

$$Re = \frac{DG_e}{\mu_e} \tag{25}$$

$$G_e = \frac{4v_e\rho_e}{\pi[D_s^2 - nD^2]} \tag{26}$$

where the pedix e is referred to the external fluid mixture and D_s is shell diameter. To calculate the contribution of radiative heat transfer, the following equations have been used:

$$h_r = \sigma\epsilon'^{\frac{(\epsilon_g T_e^4 - \alpha_g T_w^4)}{(T_e - T_w)}} \tag{27}$$

$$\epsilon' = (\epsilon_w + 1)/2 \tag{28}$$

σ is the Stefan-Boltzmann constant, while ϵ' is a correction coefficient to take into account that the surface is not black. The emissivity of the pipes (ϵ_w) was calculated by interpolation at wall temperature T_w [32,33] for AISI316 steel tubes. ϵ_g has been calculated from nomograms as a function of CO_2 and H_2O partial pressure in the gas, gas temperature T_e and the average optical path [32,33]. α_g has been calculated similarly, but it also depends on the T_w/T_e temperature ratio. Finally, T_w has been considered constant on the inner and outer skins of the pipe, because we have considered negligible resistance to heat transfer across the tube thickness, so that:

$$T_w = \frac{h_e T_e + h_i T_i}{(h_i + h_e)} \tag{29}$$

The pressure drop across the catalyst bed has been calculated according to the Ergun equation [32,33] by considering the bed porosity $\varepsilon=0.35$.

The GH2-BE-5000 prototype incorporates an ethanol catalytic combustion unit in the shell side. The rigorous modeling of this unit has not been considered essential for the purpose of this work, mainly because it was here substituted by reformate combustion to allow the use of diluted bioethanol for SRE. Therefore, in the simulation we considered an external burner for heat supply, modelled as an adiabatic Gibbs reactor.

3.3 – Fuel Cell unit

The elaboration of the fuel cell system was complicated by the need of considering the non conventional electrical output of a reactor. Therefore we modelled it as a reactor converting the reformate isothermally at 80°C, 1.8 bar.

Q and L being heat and electrical work output of the cell, we took into account the specifications of a commercial unit [34], which accounts for a 0.4 electrical efficiency. L and Q have been calculated from the enthalpy variation (ΔH) of the reactor unit called cell, obtained as output of the simulation.

3.4 – Simulation results

The output flow rates of interesting products estimated with variable H_2O/C_2H_5OH ratio are summarized in Fig. 3-6 for each reactor. These Figures may be nicely compared with H_2 concentration profiles obtained upon simulation of a similar system [8] and with the experimental ones reported for the GH_2-BE-5000 unit [18,29]. An increase of H_2 productivity is evident with increasing water feed. H_2 yield increased from 84.3% to 97.6% when increasing the water/ethanol feeding ratio from 5 to 14 (mol/mol). This can be ascribed to the promotion of the WGS reaction as testified by the corresponding decrease of CO and increase of CO_2. Therefore, the use of diluted ethanol is an effective tool to improve hydrogen yield. The decrease of CO concentration also contributes to a lower impact of the methanation reaction, which consumes H_2, further contributing to the improvement of the overall hydrogen yield, as highlighted by Fig. 7. Form this point of view the use of diluted ethanol would be the best choice to increase hydrogen productivity. However, in spite of the extensive heat exchange network introduced in the present flowsheet, aiming at decreasing the fuel consumption of the SRE reactor, a consistent heat amount is needed for that reactor, increasing with the dilution of the feed.

For the present simulations, we have chosen to thermally feed such reactor by splitting some reformate to the burner. According to the higher heat input required by SRE in the case of more diluted ethanol solutions, the reformate withdrawn from the fuel cell feed and sent to the burner increases, as shown in Fig. 8.

The power output, electrical, thermal and global, together with the relative efficiency, are reported in Table 3. According to the higher amount of reformate used as fuel to heat up the SRE reactor when diluted ethanol is fed to the plant, the fraction used in the fuel cell is lower, with consequent decrease of the electrical output and efficiency. By contrast, the thermal output increases due to a higher amount of heat made available by excess steam, which may be recovered downstream. Therefore, the electrical efficiency decreases from 0.307 at $H_2O/C_2H_5OH = 5$ (mol/mol), to 0.211 at $H_2O/C_2H_5OH = 14$ (mol/mol), while the thermal efficiency increases from 0.464 to 0.646. As a consequence, the overall efficiency of the system increases from 0.771 to 0.857, of course at the expenses of the most valuable form of energy output, *i.e.* the electrical one. The overall efficiency here reported is of course much higher than that experimentally achieved [18,29] due to substantial modification of the layout and more efficient heat integration.

The electrical efficiency here achieved was higher than what reported [35] for a similar system with SRE heating provided by ethanol combustion. Slightly different system and higher efficiency has been instead reported elsewhere [19].

At last we may conclude that the use of diluted bioethanol is technically feasible and this may open the way to a decrease of the purification costs of this biofuel with respect to its use in internal combustion engines, for which it should be heavily dehydrated. Investigations on this point have been recently summarised elsewhere [36]. Of course in this way it is compulsory to use the reformate as fuel to heat up the steam reformer, providing a different fuel or heating system for the start up of the unit. This may be feasible for stationary devices designed for continuous steady state operation. By contrast, for automotive use it is not the

right choice due to frequent start up and the need of transporting excessively diluted mixtures.

The use of diluted bioethanol improves the overall efficiency of the process due to higher heat power available, but decreases the amount of reformate which is possible to valorise in the fuel cell to produce electrical power. Therefore, these parameters should be taken into account in the economic evaluation of the solution.

4 - CONCLUSIONS

A system was evaluated for the electrical and thermal cogeneration from bioethanol. The apparatus is constituted by a fuel processor, including a steam reformer, two water gas shift and a methanation reactors in series, and a PEM fuel cell. The target power is nominally 5 kW_{el} + 5 kW_{th}, amenable for residential cogeneration.

In the present work, different layouts have been tested, trying in particular to optimise the heat exchange network. The possibility to operate with diluted ethanol solutions has been checked, opening the way to lighter purification strategies for bioethanol, with decreasing production cost. Therefore, the water/ethanol feeding ratio was the main parameter varied in process simulation, in order to check its effect on the operation of the reactors and on power output and efficiency. Heat supply to the reformer was accomplished by feeding part of the reformate to a burner.

H_2O/C_2H_5OH was varied between 5 and 14 mol/mol. H_2 yield increased with increasing this parameter. However, more diluted solutions required higher heat input to the SRE reactor, imposing to withdraw a higher fraction of the reformate from the fuel cell. As a consequence, the electrical output and efficiency decreased. However, heat remained available in residual steam, which may be recovered effectively and used, increasing the thermal output and efficiency, with a global increase of the overall plant efficiency.

In conclusion, the use of diluted bioethanol may be envisaged for H_2 production, provided that sufficient heat is furnished to the steam reforming reactor by burning part of the reformate. If electrical output is the most valuable goal, it is better to operate with the lowest water/ethanol ratio, whereas at higher dilution the thermal output and plant efficiency may be maximised.

REFERENCES

1. V. A. Kirillov, V. D. Meshcheryakov, V. A. Sobyanin, V. D. Belyaev, Yu. I. Amosov, N. A. Kuzin, A. S. Bobrin, Theoretical Foundations of Chemical Engineering, 42 (2008) 1.

2. F. Díaz Alvarado, F. Gracia, Chem. Eng. J., 165 (2010) 649.

3. M. Ni, D.Y.C. Leung, M.K.H. Leung, Int. J. Hydrogen Energy, 32 (2007) 3238.

4. http://betarenewables.neencloud.it/proesa/what-is

5. T. Aicher, J. Full, A. Schaadt, Int. J. Hydrogen Energy, 34 (2009) 8006.

6. S. Biset, L. Nieto Deglioumini, M. Basualdo, V.M. Garcia, M. Serra, J. Power Sources, 192 (2009) 107.

7. L. Nieto Degliuomini, D. Zumoffen, M. Basualdo, Int. J. Hydrogen Energy, 37 (2012) 14801.

8. L. Nieto Degliuomini, S. Biset, P. Luppi, M.S. Basualdo, Int. J. Hydrogen Energy, 37 (2012) 3108.

9. J.H. Oakley, A.F.A. Hoadley, Int. J. Hydrogen Energy, 35 (2010) 8472.

10. L. Hernández, V. Kafarov, J. Power Sources, 192 (2009) 195.

11. U.W. Hartley, S. Amornraksa, P. Kim-Lohsoontorn, N Laosiripojana, Chem. Eng. J. 278 (2015) 2.

12. T. Hou, S. Zhang, T. Xu, W. Cai, Chem. Eng. J., 255 (2014) 149.

13. J. Thormann, P. Pfeifer, U. Kunz, Chem. Eng. J., 191 (2012) 410.

14. I. Uriz, G. Arzamendi, E. Lopez, J. Llorca, L.M. Gandìa, Chem. Eng. J., 167 (2011) 603.

15. Y.S. Cheng, M.A. Pena, K.L. Yeung, J. Taiwan Institute of Chem Eng., 40 (2009) 281.

16. K.L. Yeung, R. Aravind, J. Szegner, A. Varma, Stud. Surf. Sci. Catal., 101 (1996) 1349.

17. D. Montané, E. Bolshak, S. Abelló, Chem. Eng. J., 175 (2011) 519.

18. I. Rossetti, C. Biffi, G.F. Tantardini, M. Raimondi, E. Vitto, D. Alberti, Int. J. Hydrogen Energy, 37 (2012) 8499.

19. P. Giunta, C. Mosquera, N. Amadeo, M. Laborde, J. Power Sources, 164 (2007) 336.

20. E. Verykios, U.S. Patent No. 6,605,376 (2003), to Helbio S.A.

21. W. Jamsak, P.L. Douglas, E. Croiset, R. Suwanwarangkul, N. Laosiripojana, S. Charojrochkul, S. Assabumrungrat, J. Power Sources, 187 (2009) 190.

22. M. De Falco, F. Gallucci, Int. J. Hydrogen Energy, 35 (2010) 3463.

23. V.M. García, E. López, M. Serra, J. Llorca, J. Power Sources 192 (2009) 208.

24. Y.M. Bruschi, E. Lòpez, N. S. Schbib, M.N. Pedernera, D.O. Borio, Int. J. Hydrogen Energy, 37 (2012) 14887.

25. T.L. LeValley, A.R. Richard, M. Fan, Int. J. Hydrogen Energy, 39 (2014) 16983.

26. A. Mishra, R. Prasad, Bull. Chem. React. Eng. & Catal., 6 (2011) 1.

27. D.L. Trimm, Appl. Catal. A: General, 296 (2005) 1.

28. P. Djinovic, C. Galletti, S. Specchia, V. Specchia, Catal. Today, 164 (2011) 282.

29. I. Rossetti, C. Biffi, L. Forni, G.F. Tantardini, G. Faita, M. Raimondi, E. Vitto, D. Alberti, Proceedings of the ASME 2010 Eight International Fuel Cell Science, Engineering and Technology Conference, FuelCell2010, June 14-16, 2010, Brooklyn, New York, USA, 2 (2010) 465.

30. C. Graschinsky, M. Laborde, N. Amadeo, A. Le Valant, N. Bion, F. Epron, D. Duprez, Ind. Eng. Chem. Res., 49 (2010) 12383.

31. V. Mas, M.L. Bergamini, G. Baronetti, N. Amadeo, M. Laborde, Top. Catal., 51 (2008) 39.

32. H. Scott Fogler, "Elements of Chemical Reaction Engineering", IV Edition, Ed. Prentice Hall.

33. Fenomeni di Trasporto, L. Forni, I. Rossetti, Ed. Cortina, 2009.

34. www.horizonfuelcell.com.

35. J.A. Francesconi, M.C. Mussati, R.O. Mato, P.A. Aguirre, J. Power Sources, 167 (2007) 151.

36. I. Rossetti, J. Lasso, M. Compagnoni, G. De Guido, L. Pellegrini, Chem. Eng. Trans., 43 (2015) 229.

TABLES

Table 1: Results of Model 3 implementation and estimated kinetic and adsorption parameters.

Model 3									
	mol s^{-1} g^{-1}			J mol^{-1}					J mol^{-1}
k_{05}	1.544E+20		Ea$_5$	302980		C$_0$	2.926E-02	ΔH_C	-55199
k_{07}	1.920E+05		Ea$_7$	41605		F$_0$	2.412E-04	ΔH_F	-76661
k_{013}	7.756E+09		Ea$_{13}$	187783		G$_0$	9.940E+01	ΔH_G	-13965
k_{014}	5.044E+05		Ea$_{14}$	56252		H$_0$	2.322E+00	ΔH_H	27945
						I$_0$	4.907E-02	ΔH_I	-67738
						M$_0$	1.369E-01	ΔH_M	-32808
						N$_0$	1.660E-05	ΔH_N	16489

Table 2: Sizing details of the optimized reformer reactor used for the simulations

Spatial distribution	Triangular network
Tubes number	109
Tube lenght	510 mm
Tube diameter	12 mm
Interaxial distance	16.16 mm
Shell internal diameter	190 mm
Material	AISI 316

Table 3: Electrical and thermal power output as a result of simulations with variable water/ethanol feeding ratio. Plant efficiency calculated with respect to the lower heating value of ethanol.

H₂O/C₂H₅OH inlet (mol/mol)	5	6.5	8.5	11	14
ΔH of the cell [W]	14771	14583	13745	12626	10845
Thermodynamic efficiency	0.434	0.431	0.429	0.427	0.425
Electric power output of the cell [W]	6417	6288	5895	5386	4609
Power used by PUMP and Compressor [W]	613.	614.0	614.2	614.6	614.9
Net electric output [W]	5803	5674	5281	4772	3994
Thermal power output of the cell [W]	8353	8296	7850	7239	6236
Thermal power absorbed by H₂O in COND [W]	436	1315	2564	4099	5996
Total thermal power [W]	8790	9610	10413	11339	12233
Power loss[a] [W]	6452	5761	5351	4935	4818
Electric efficiency[b]	0.307	0.300	0.279	0.252	0.211
Thermal efficiency[b]	0.464	0.508	0.550	0.599	0.646
Total efficiency[b]	0.771	0.807	0.829	0.851	0.857

a) Referred to the ΔH of combustion of C_2H_5OH at 15 °C, to produce CO_2 and H_2O liquid at 15 °C = 1372.5 kJ mol⁻¹.
b) Referred to the lower heating value of pure C_2H_5OH = 1234.8 kJ mol⁻¹.

FIGURES

Fig. 1: Schematic representation of process layout, including a basic representation of heat flows, for (a) the experimental GH2 -BE- 5000 apparatus and (b) the simplified, heat integrated system proposed for the present simulations.
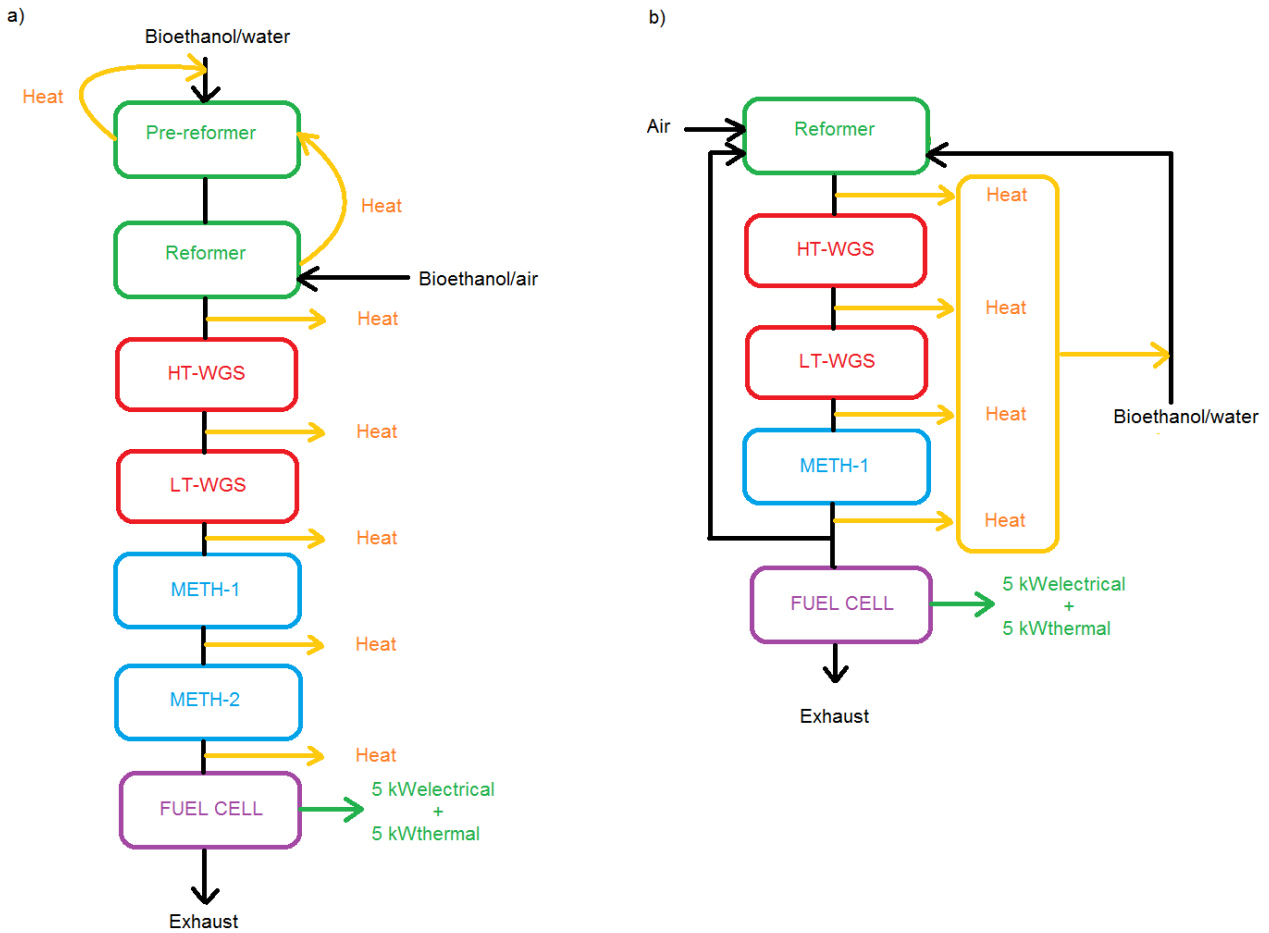
Fig. 2: Flowsheet of the simulated CHP unit. Material streams are indicated with continuous lines, heat flow with dotted lines. I = input, O = output of the relative reactor.
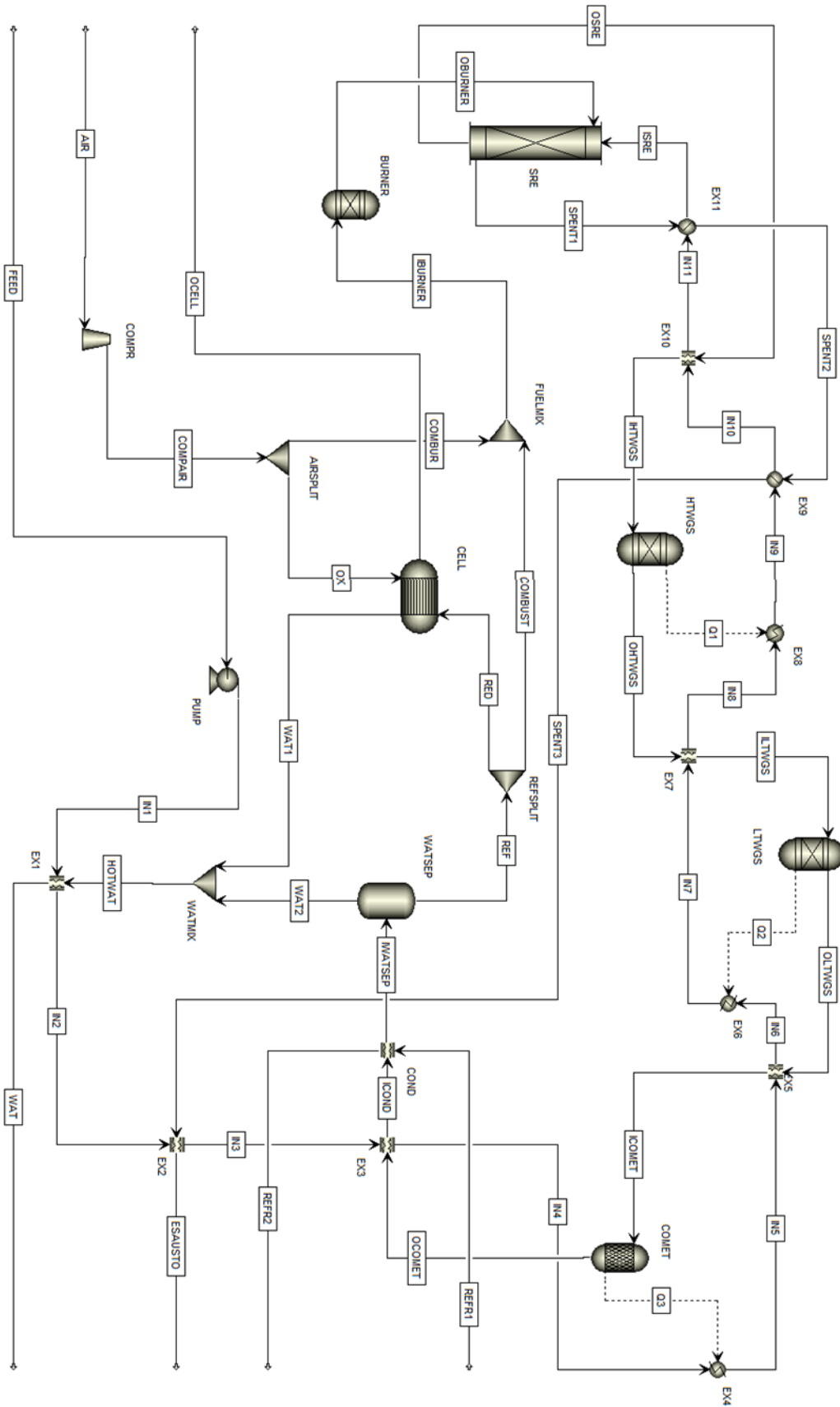
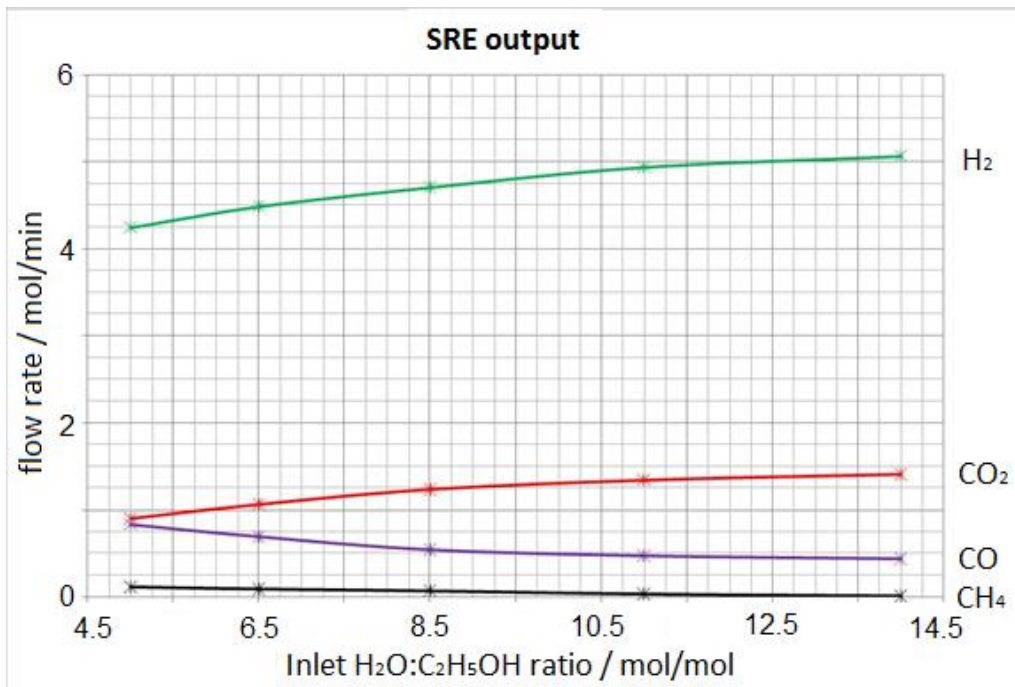**Fig. 3:** Molar flow rate of different products outflowing the SRE reactor at different inlet H_2O/ethanol ratio.
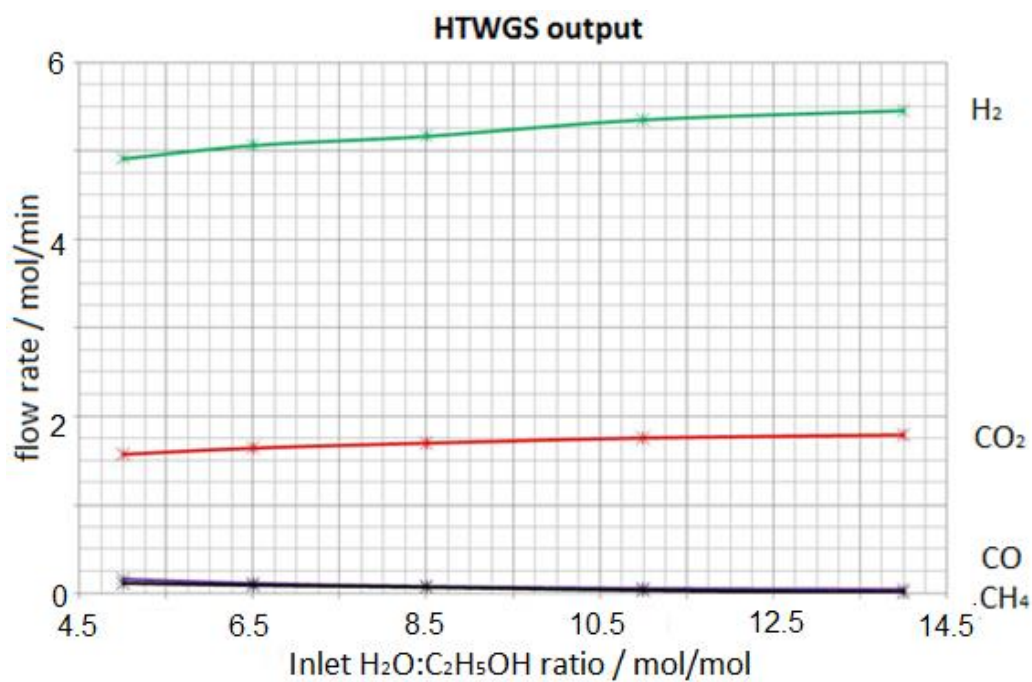

Fig. 4: Molar flow rate of different products outflowing the HTWGS reactor at different inlet H_2O/ethanol ratio.

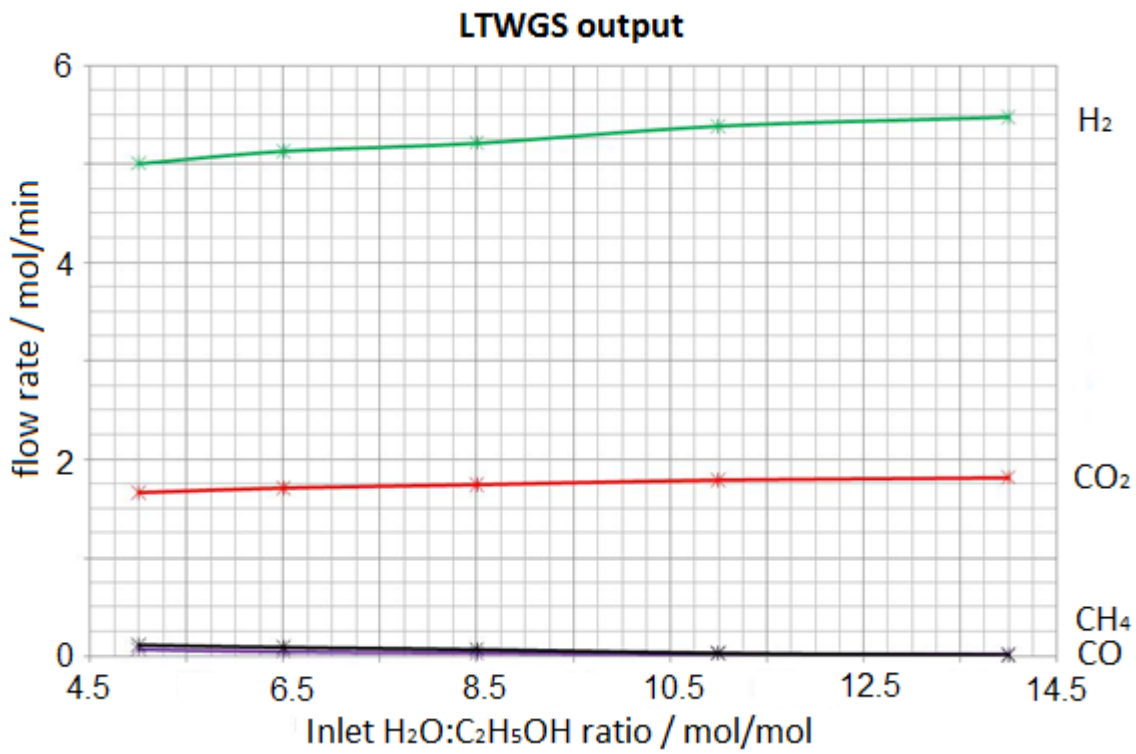**Fig. 5:** Molar flow rate of different products outflowing the LTWGS reactor at different inlet H_2O/ethanol ratio.

LTWGS output

flow rate / mol/min

Inlet H_2O:C_2H_5OH ratio / mol/mol

H_2

CO_2

CH_4
CO

Fig. 6: Molar flow rate of different products outflowing the COMETH reactor at different inlet H_2O/ethanol ratio.

METH output

flow rate / mol/min

Inlet H_2O:C_2H_5OH ratio / mol/mol
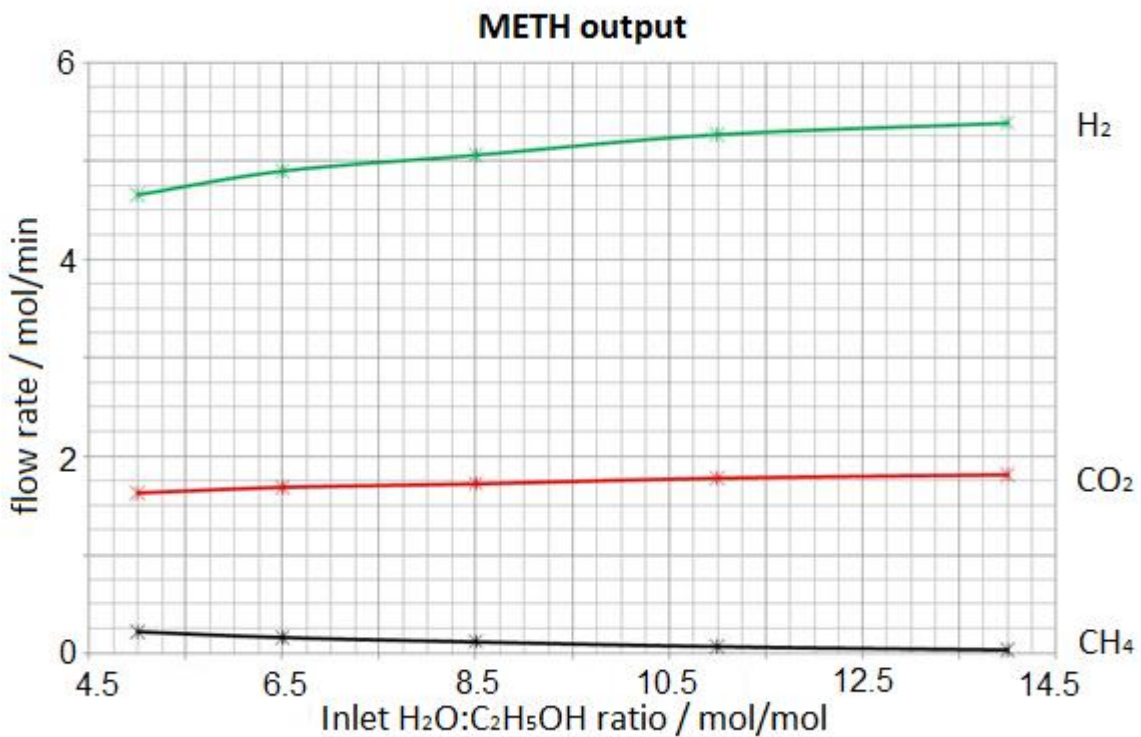
H_2

CO_2

CH_4

Fig. 7: H_2 flowrate trend after different reactors as a function of inlet water/ethanol ratio (increasing in the sense of the arrow).

H₂ flow rate in the outlet of various reactors

Legend:
- H2O/C2H5OH=14
- H2O/C2H5OH=11
- H2O/C2H5OH=8,5
- H2O/C2H5OH=6,5
- H2O/C2H5OH=5

y-axis: H_2 flowrate / mol/min (4.2, 4.5, 4.8, 5.1, 5.4)
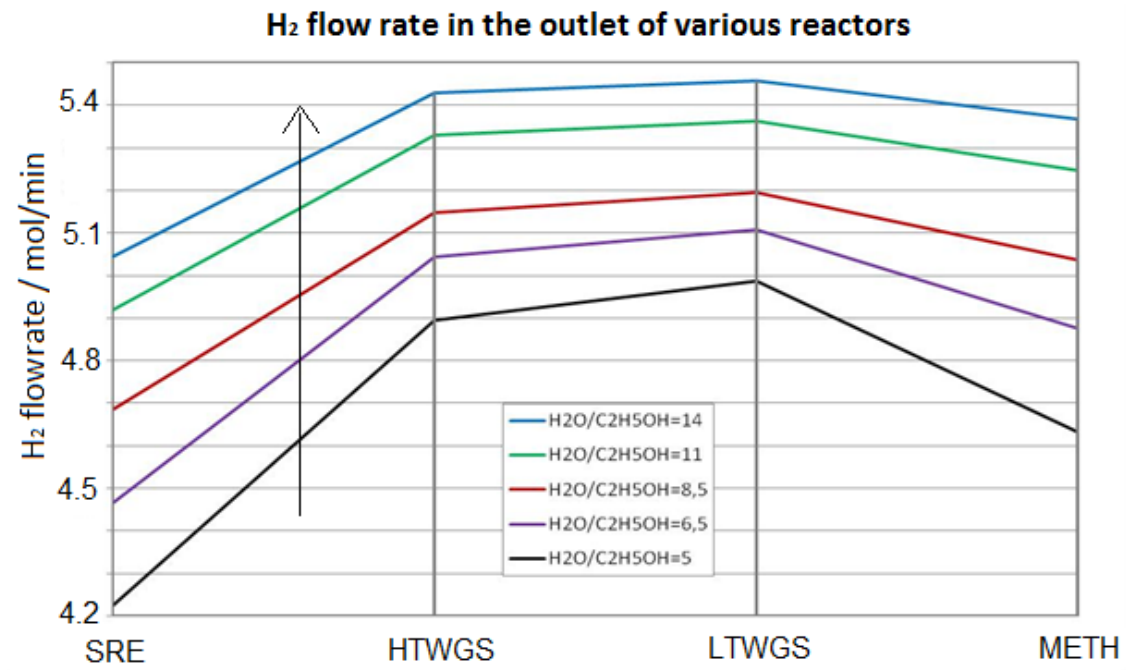
x-axis: SRE, HTWGS, LTWGS, METH

Fig. 8: H_2 flowrate produced and fed to the fuel cell as a function of inlet water/ethanol ratio.

y-axis: flow rate / mol/min (0, 2, 4, 6)

x-axis: Inlet H_2O:C_2H_5OH ratio / mol/mol (4.5, 6.5, 8.5, 10.5, 12.5, 14.5)

H_2 produced

H_2 fed to FC